

Long-range atmospheric transport of polycyclic aromatic hydrocarbons: A global 3-D model analysis including evaluation of Arctic sources

SUPPORTING INFORMATION

Carey L. Friedman^{§*} and Noelle E. Selin[†]

Massachusetts Institute of Technology, Cambridge, Massachusetts, 02139 USA

*Corresponding author e-mail: clf@mit.edu

[§]Center for Global Change Science, Massachusetts Institute of Technology, Cambridge, Massachusetts, 02139 USA

[†]Engineering Systems Division and Department of Earth, Atmospheric, and Planetary Sciences, Massachusetts Institute of Technology, Cambridge, Massachusetts, 02139 USA

Contents

Parameterization of temperature dependent gas-particle partitioning	S2
OC and BC aerosol concentrations	S2
Gas phase OH oxidation schemes	S2-S3
On-particle O ₃ oxidation schemes	S3
Table S1: Physicochemical constants used in model for PHE, PYR, and BaP	S4
Table S2: Overall lifetimes and lifetimes due to different processes for PHE, PYR, and BaP	S4
Figure S1: Simulated vs. measured PHE, PYR, and BaP scatter plot of data from main text Table 1	S5
Figure S2: Geometric seasonal mean nonurban mid-latitude concentrations	S6
Figure S3: Geometric seasonal mean Arctic concentrations	S7
Figure S4: Simulated vs. measured PHE, PYR, and BaP at urban locations	S8
Figure S5: GEOS-Chem global budget for PHE, PYR, and BaP	S9
Figure S6: Seasonal wet and dry deposition of PHE, PYR, and BaP	S10
Figure S7: Annual wet and dry deposition of PHE, PYR, and BaP	S11
Figure S8: Simulated vs. measured BaP with simulations conducted using both hydrophobic and hydrophilic aerosol scavenging efficiencies	S12
Figure S9: Simulated vs. measured PHE, PYR, and BaP at Spitsbergen, NO (2005)	S13
Figure S10: Simulated vs. measured PHE, PYR, and BaP at Spitsbergen, NO (2006)	S14
Figure S11: Simulated (both 4°×5° and 2°×2.5° spatial resolution) vs. measured PHE, PYR, and BaP at Spitsbergen, NO (2008)	S15
Figure S12: Simulated (both 4°×5° and 2°×2.5° spatial resolution) vs. measured PHE, PYR, and BaP at Spitsbergen, NO (2009)	S16
Literature cited	S17

Temperature dependence of gas-particle partitioning

We incorporate K_{OA} temperature dependence into the default model according the van't Hoff relationship:

$$K_{OA}(T_2) = K_{OA}(T_1) \cdot e^{-\frac{\Delta_{OA}H}{R} \left(\frac{1}{T_2} - \frac{1}{T_1} \right)} \quad (\text{Eq. S1})$$

where T_1 is 298 K and T_2 is ambient atmospheric temperature (K), R is the ideal gas constant ($\text{J mol}^{-1} \text{K}^{-1}$), and $\Delta_{OA}H$ is the enthalpy of phase change from air to octanol (J mol^{-1}), estimated from the enthalpy of phase change from the pure liquid state to the gas phase¹. Values of K_{OA} and $\Delta_{OA}H$ are provided below in Table S1.

OC and BC aerosol concentrations

Monthly mean OC and BC aerosol concentrations were simulated with GEOS-Chem separately from PAHs for the year 2008. Monthly mean OC and BC concentrations were then used as input to all years of the default PAH simulation. Therefore, there was no interannual variability in OC/BC. Minimum monthly OC concentrations ranged from 0 ng C m^{-3} (Feb., Sep., Oct.) to $4.2\text{E}-12 \text{ ng C m}^{-3}$ (March), while maximum concentrations ranged from $1.2\text{E}+4 \text{ ng C m}^{-3}$ (Nov.) to $1.7\text{E}+5 \text{ ng C m}^{-3}$ (June). Minimum BC concentrations ranged from 0 ng C m^{-3} (June) to $4.4\text{E}-12 \text{ ng C m}^{-3}$ (August) and maximum concentrations ranged from $4.0\text{E}+3 \text{ ng C m}^{-3}$ (Dec.) to $3.8\text{E}+4 \text{ ng C m}^{-3}$ (June).

OH oxidation

Standard simulations have a temperature-independent k_{OH} , but a temperature-dependent k_{OH} sensitivity analysis was conducted for PHE, with k_{OH} determined by the Arrhenius expression:

$$k_{OH} = A \exp\left(\frac{-E_a}{RT}\right) \quad (\text{Eq. S2})$$

where the pre-exponential factor (A) and the activation energy (E_a) are from Brubaker and Hites². Empirically determined A and E_a are unavailable for PYR and BaP.

On-particle O₃ oxidation schemes

Pöschl reaction scheme: According to Pöschl et al. (2001)³, the reaction of soot particulate BaP with ozone (O₃) will proceed at rate k (s⁻¹):

$$k = k_{\max} (K_{O_3})[O_3]/(1 + K_{O_3}[O_3]) \quad (\text{Eq. S3})$$

where k_{\max} is the maximum pseudo-first-order BaP decay rate coefficient in the limit of high O₃ concentrations (s⁻¹); K_{O_3} is the Langmuir adsorption equilibrium constant for O₃ (cm³), and [O₃] is the ambient ozone concentration (molec/cm³). Pöschl et al. determined that for oxidation of BaP on spark discharge soot particles at 296 K and 1 atm, $k_{\max} = 0.015 \pm 0.001$ s⁻¹ and $K_{O_3} = (2.8 \pm 0.2) \times 10^{-13}$ cm³.

Kahan reaction scheme: Kahan et al. (2006)⁴ follow the same general reaction scheme, but fit an observed k_{O_3} to an equation of the form:

$$k_{obs} = \frac{A \times [O_3(g)]}{B + [O_3(g)]} \quad (\text{Eq. S4})$$

and find that for the ozonation of surface BaP dissolved in octanol, $A = (5.5 \pm 0.2) \times 10^{-3}$ s⁻¹ and $B = (2.8 \pm 0.4) \times 10^{15}$ molec/cm³.

Kwamena reaction scheme: Kwamena et al. (2004)⁵ follow the same equation as Pöschl et al. and find that for oxidation of BaP on azelaic acid aerosols at 72% relative humidity, $k_{\max} = 0.060 \pm 0.018$ s⁻¹ and $K_{O_3} = (2.8 \pm 1.4) \times 10^{-15}$ cm³

TABLES

Parameter	Description	PHE	PYR	BaP	References
$\log K_{OA}$	Octanol-air partition coefficient	7.64	8.86	11.48	1
$\log K_{BC}$	Black carbon-air partition coefficient	10.0	11.0	13.9	2
$\Delta_{OA}H$ (kJ/mol)	Enthalpy of phase transfer from gas phase to OC	-74	-87	-110	3
$\Delta_{BC}H$ (kJ/mol)	Enthalpy of phase transfer from gas phase to BC	-74	-87	-110	3
k_{OH} (cm ³ /molec/s)	Reaction rate constant for oxidation of gas phase with OH	2.70×10^{-11} , 1.30×10^{-11}	5.00×10^{-11}	5.00×10^{-11}	4, 5
A (cm ³ /s)	Pre-exponential factor (Arrhenius equation)	14×10^{-12}	—	—	4
E_a (J/mol)	Activation energy	-1.6×10^3	—	—	4
$\log K_{AW}$	Air-water partition coefficient	-2.76	-3.27	-4.51	1
$\Delta_{AW}H$ (kJ/mol)	Enthalpy of phase transfer from water to air	-47	-43	-43	3
ρ_{oct} (kg/m ³)	Density of octanol	820			2
ρ_{BC} (kg/m ³)	Density of BC	1000			2

Table S1. Physicochemical constants used in model for PHE, PYR, and BaP. References: (1) Ma et al., 2010⁶; (2) Lohmann and Lammel, 2004⁷; (3) Schwarzenbach et al., 2003¹; (4) Brubaker and Hites, 1998², (5) U.S. EPA Episuite software⁸.

		Lifetime (days):			
PAH	Phase	Oxidation	Wet deposition	Dry deposition	Overall
PHE	Gas	0.18	45	0.83	0.15
	OC	—	11	2.4	0.30
	BC	—	8.4	3.0	0.20
	Total				0.15
PYR	Gas	0.14	20	0.33	0.10
	OC	—	14	2.4	0.26
	BC	—	9.2	3.4	0.16
	Total				0.11
BaP	Gas	0.017	0.67	0.11	0.12
	OC	—	3.8	1.8	0.35
	BC	—	4.2	2.3	0.23
	Total				0.23

Table S2. Lifetimes (days) of gas, OC- and BC-phase PHE, PYR, and BaP against oxidation and wet and dry deposition, and total PHE, PYR, and BaP lifetimes. The calculation of overall lifetimes for each phase include loss and addition due to reversible partitioning (individual lifetimes due to partitioning not shown).

FIGURES

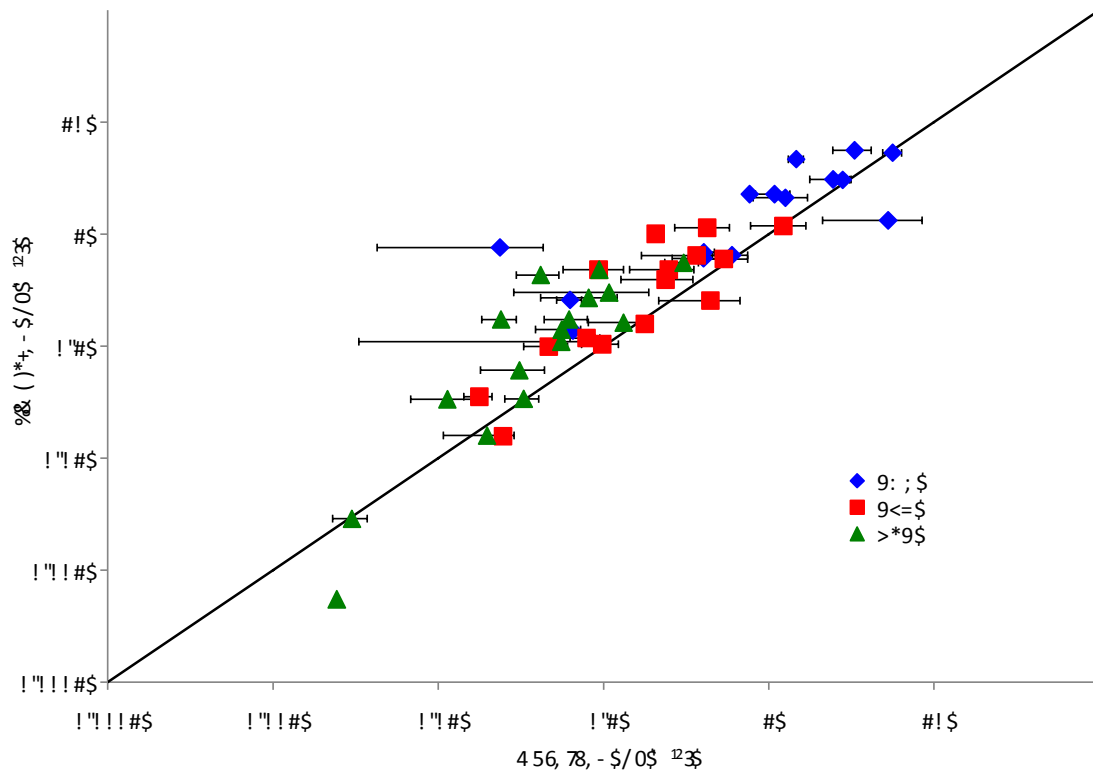


Figure S1. Simulated versus observed concentrations (ng m^{-3}) for PHE (blue diamonds), PYR (red squares), and BaP (green triangles) for all nonurban stations shown in Table 1 in the main text. The one-to-one line is shown in black. The fitted linear equations are $y = 0.65x + 1.09$ (PHE, $n = 15$); $y = 0.93 + 0.19$ (PYR, $n = 15$); $y = 1.78x + 0.07$ (BaP, $n = 16$).

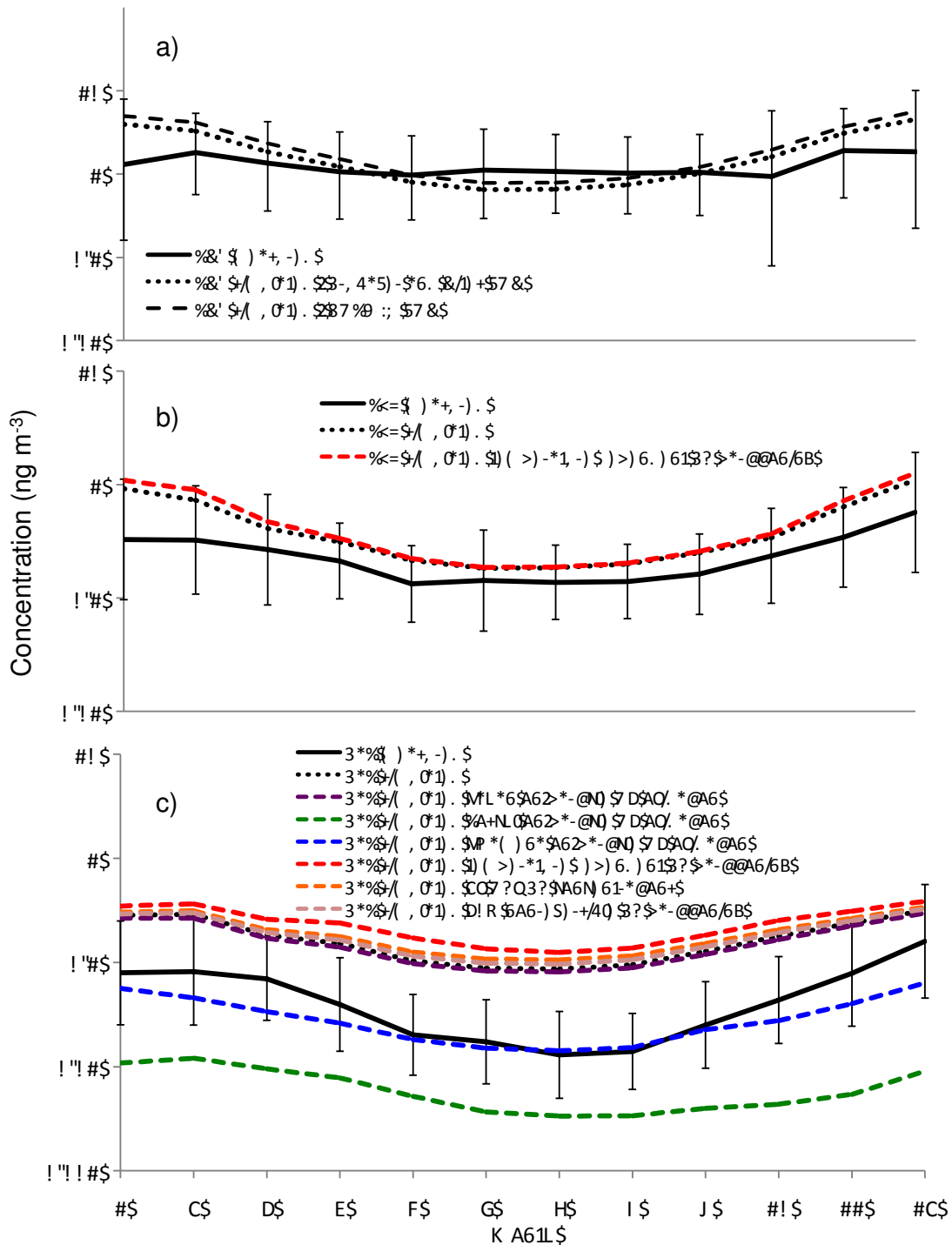


Figure S2. Nonurban mid-latitude geometric mean total concentration (gas + particle) seasonal variation from sites/years listed in Table 1 (observed; solid black line) and for simulated years 2005-2009 (modeled; dotted black line) for a) PHE, b) PYR, and c) BaP. Error bars are \pm one geometric standard deviation of monthly means across sites. Colored lines represent results from sensitivity analyses. Simulated and observed data are identical to those shown in Figure 2 in the main text.

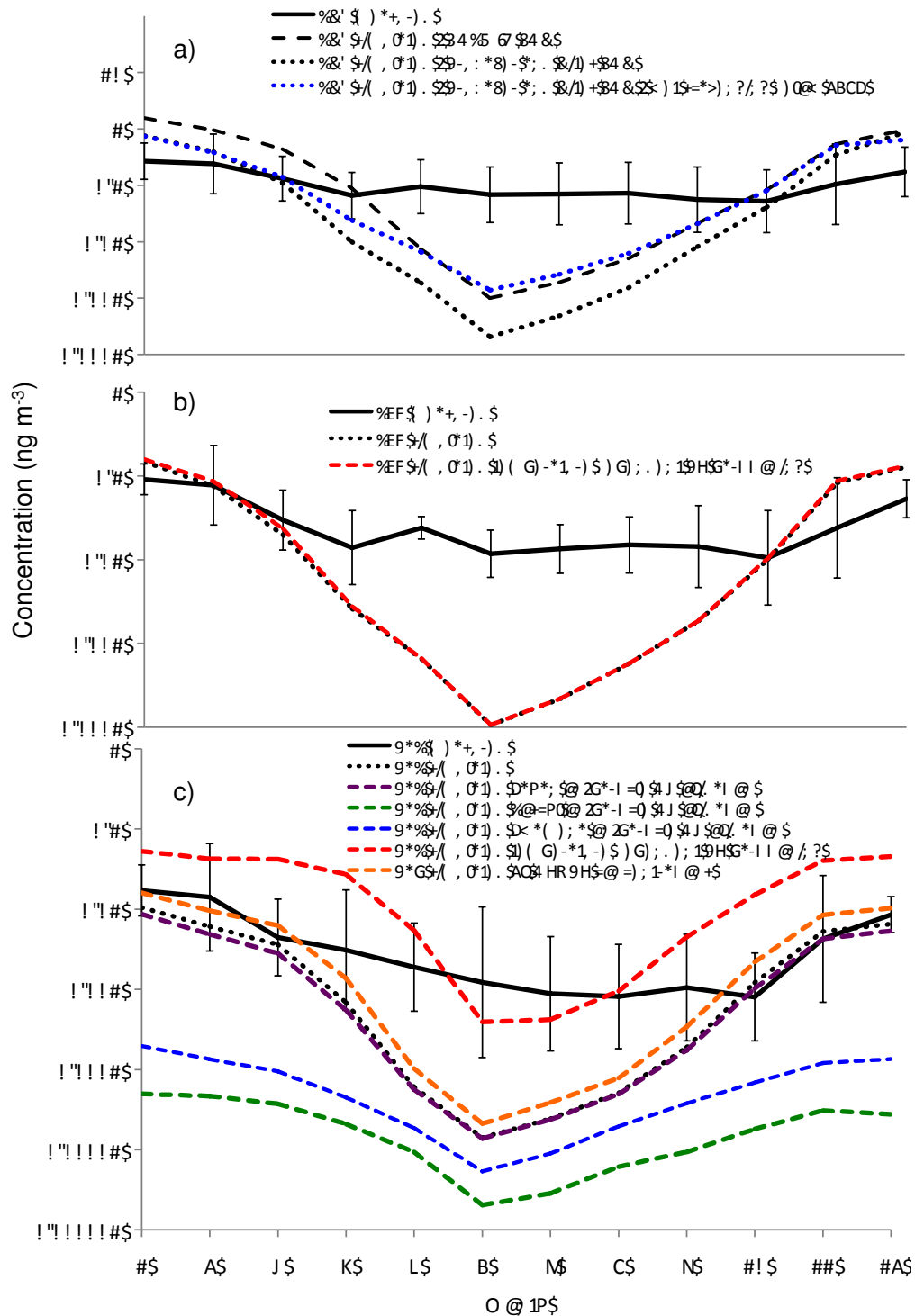


Figure S3. Arctic geometric mean total concentration (gas + particle) seasonal variation from sites/years listed in Table 1 (observed) and for simulated years 2005-2009 (modeled) for (a) PHE, (b) PYR, and (c) BaP. Error bars are \pm one geometric standard deviation of monthly means across sites. Colored lines represent results from sensitivity analyses. Simulated and observed data are identical to those shown in Figure 3 in the main text.

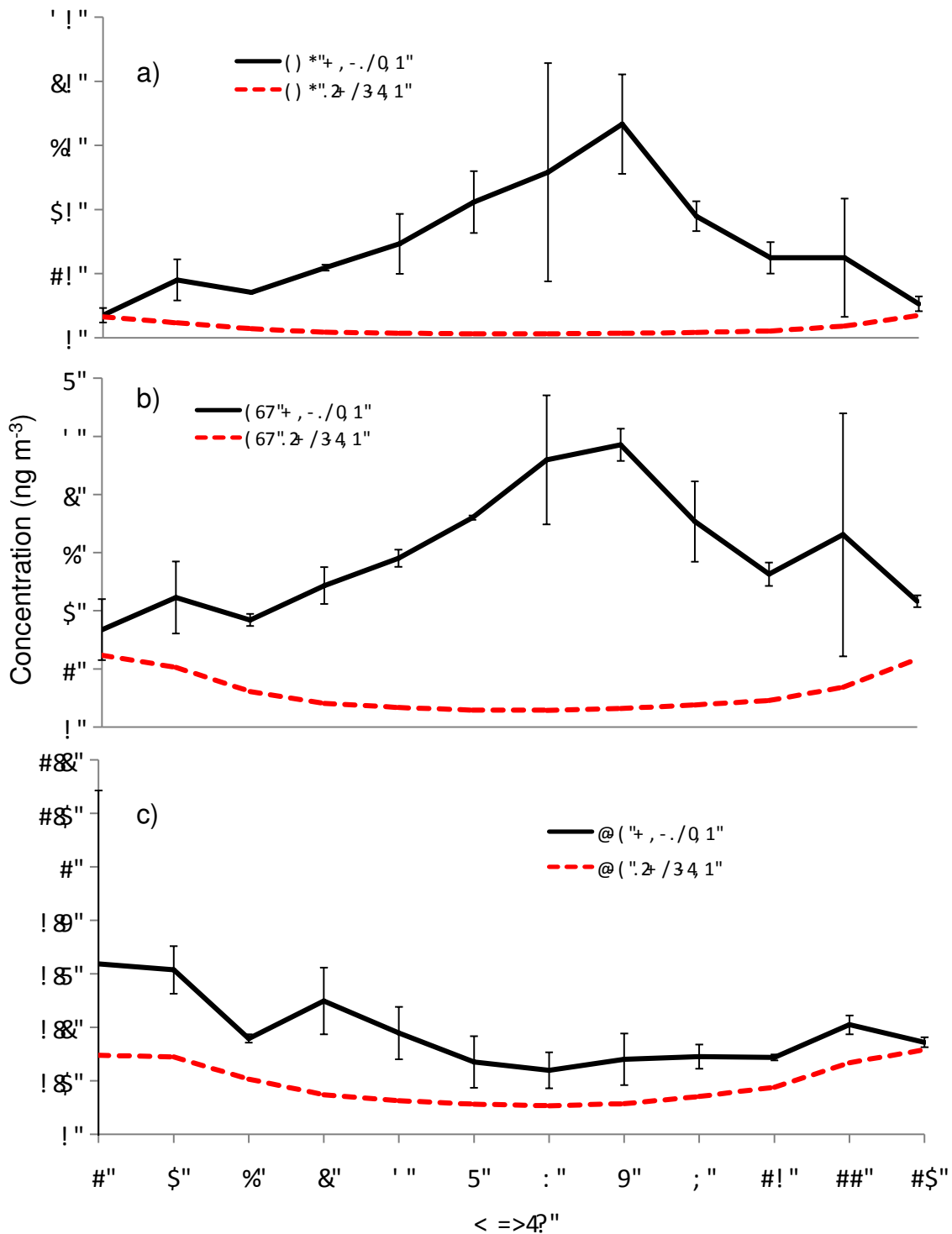


Figure S4. Mean seasonal total concentrations (ng m^{-3}) of a) PHE, b) PYR, and c) BaP at two urban stations (also Great Lakes stations): Sturgeon Point, New York, USA, and Cleveland, Ohio, USA. The figure demonstrates that GEOS-Chem underpredicts concentrations at urban locations and does not capture the summer-time maximum for PHE and PYR.

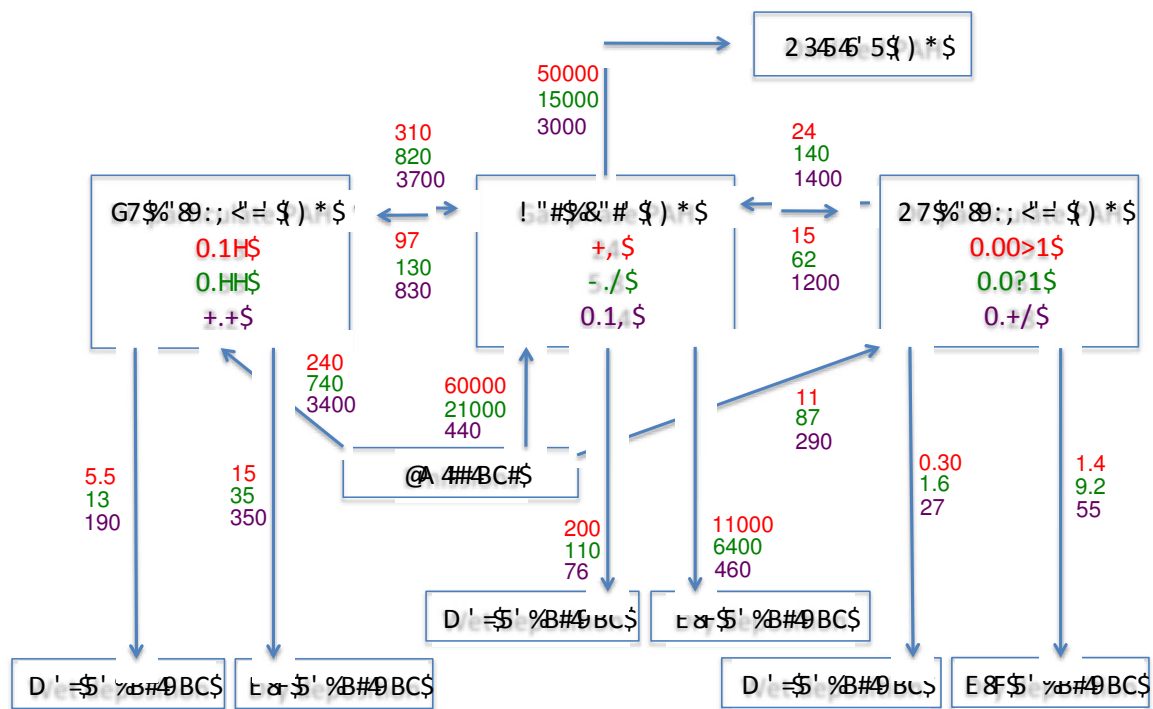


Figure S5. Global budget of atmospheric PHE (red), PYR (green), and BaP (purple) in GEOS-Chem. Inventories are in Mg (boxes) and rates are in Mg yr⁻¹ (arrows).

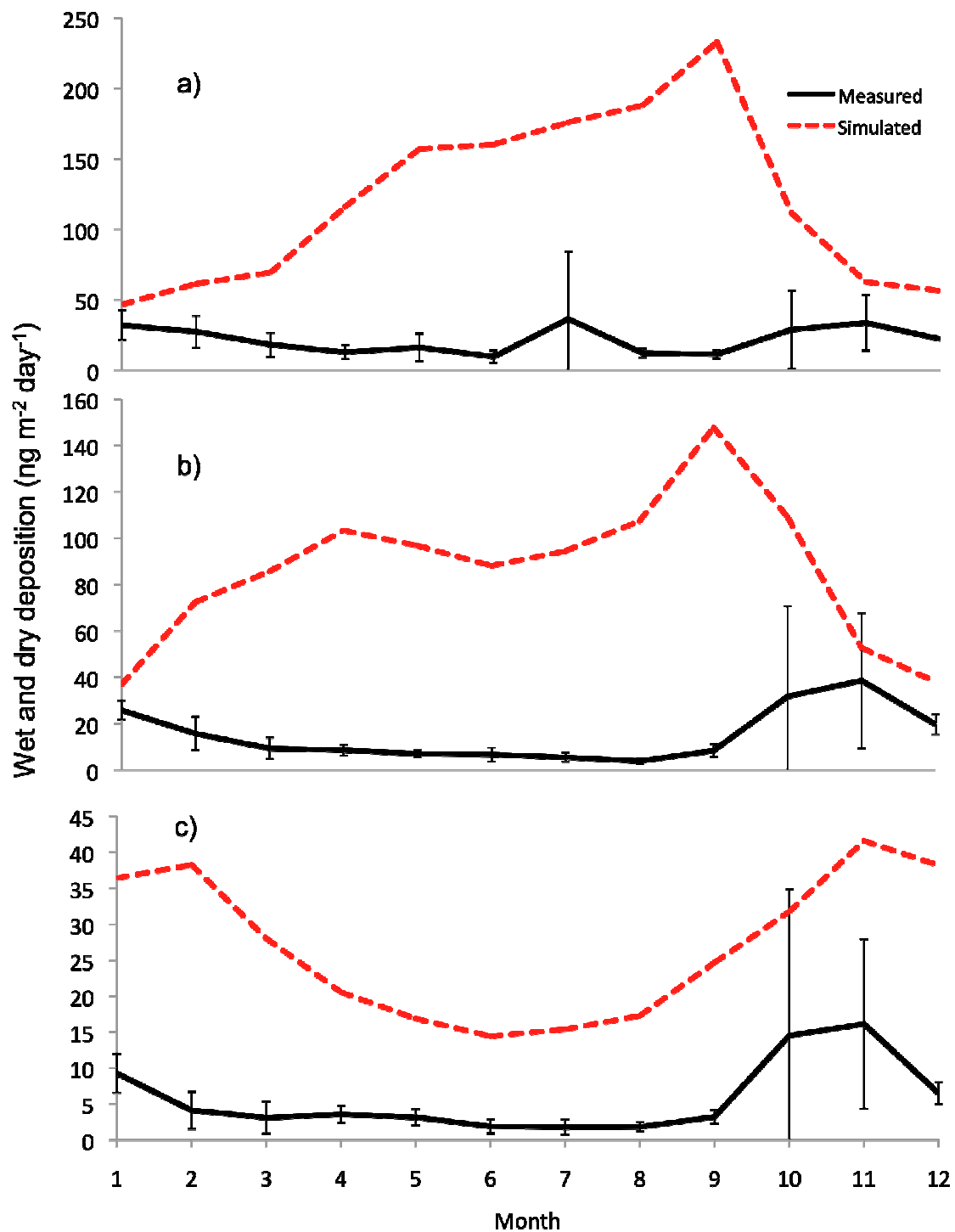


Figure S6. Mean seasonal total deposition (wet and dry combined) of a) PHE, b) PYR, and c) BaP observed at three northern European stations (solid line; see Table 1 in main text) and mean modeled total deposition (dotted line) from same sites. Modeled deposition was determined with a hydrophobic aerosol scavenging rate applied to particulate PAHs. Error bars are \pm one standard deviation of monthly means across sites.

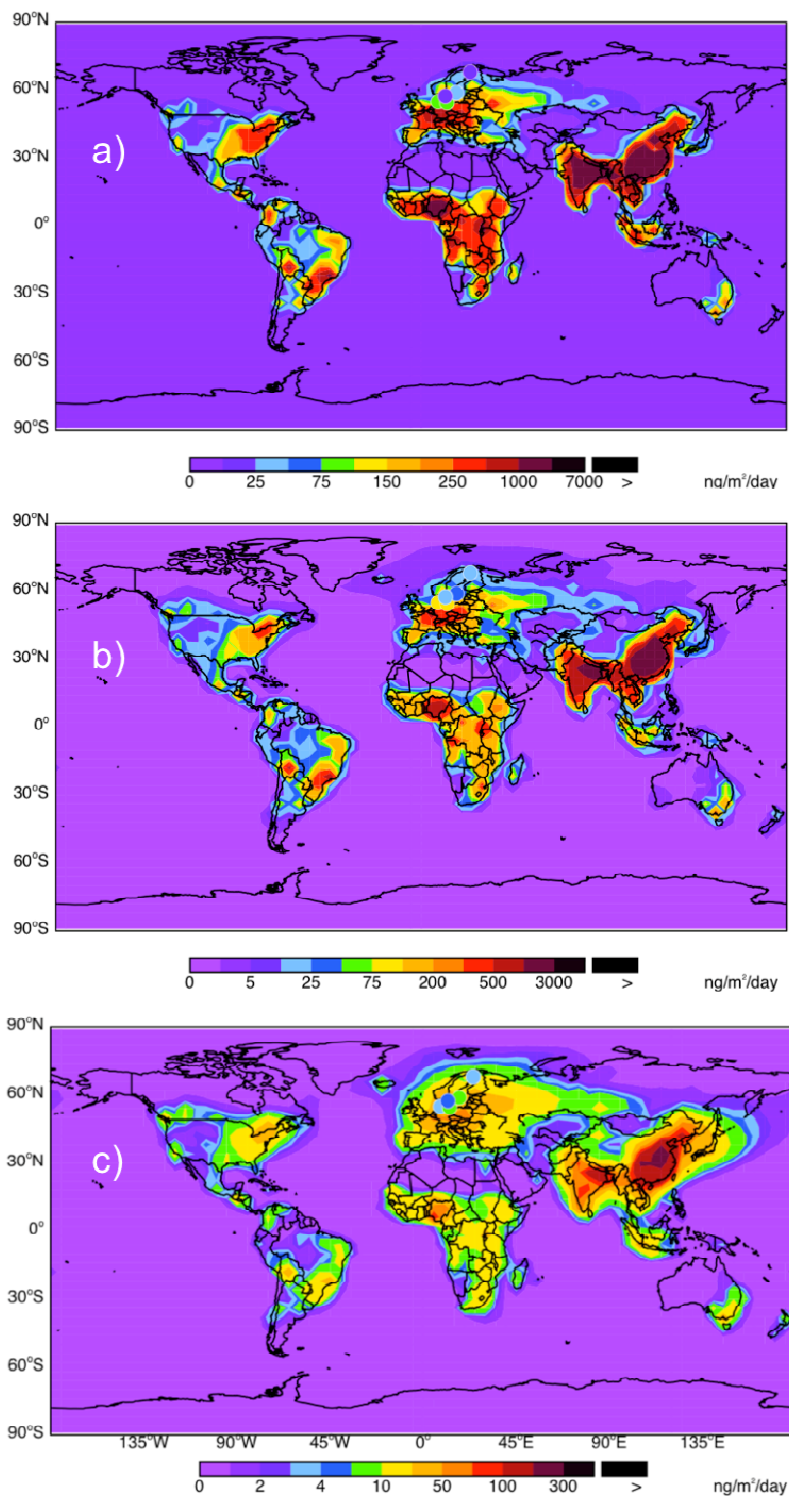


Figure S7. Mean annual PHE (a), PYR (b), and BaP (c) total (wet + dry) simulated concentrations in surface air from 2005-2009 (background). Land-based observations for deposition from Table 1 are shown with circles. Observations from long-term monitoring stations are inter-annual means for the years shown in Table 1.

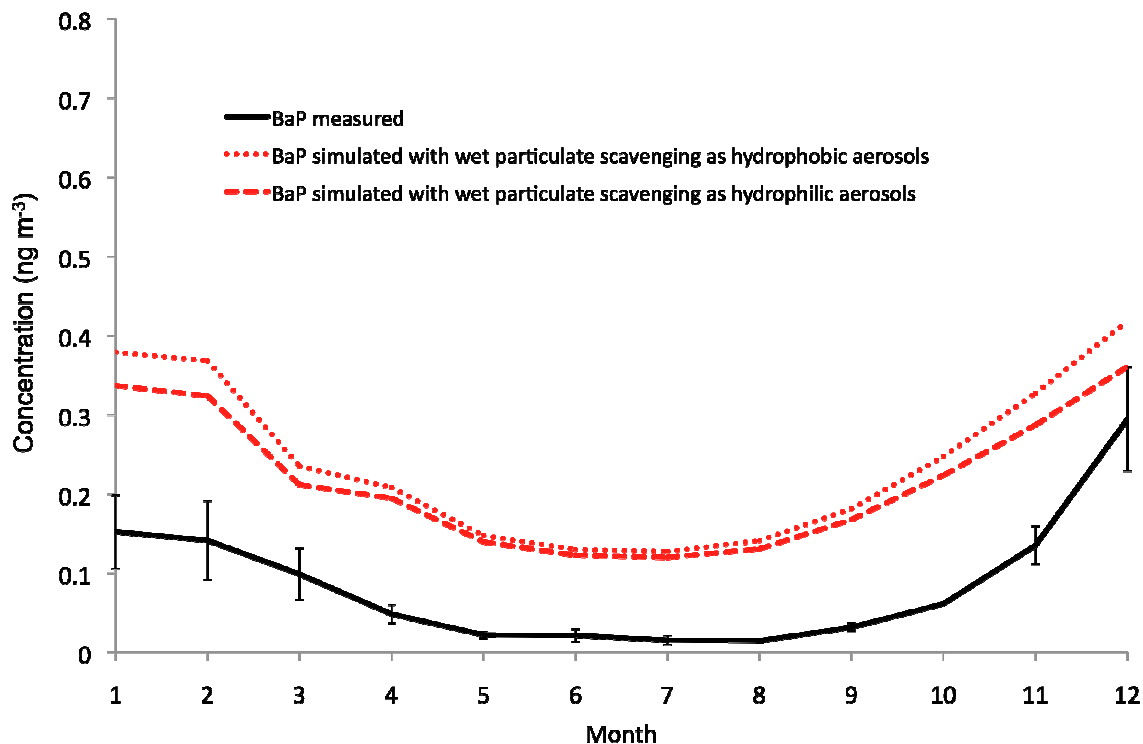


Figure S8. Simulated concentrations of BaP at non-urban mid-latitude locations using both the default particulate wet deposition scavenging efficiency, i.e., as hydrophobic aerosols, and scavenging with a hydrophilic aerosol efficiency. Also shown are observed BaP concentrations. Applying a hydrophilic scavenging efficiency results in a small decrease in mean atmospheric total BaP concentrations. Changing the particulate scavenging rate efficiency had no effect on PHE or PYR concentrations. Error bars are +/- one standard deviation of monthly means across sites.

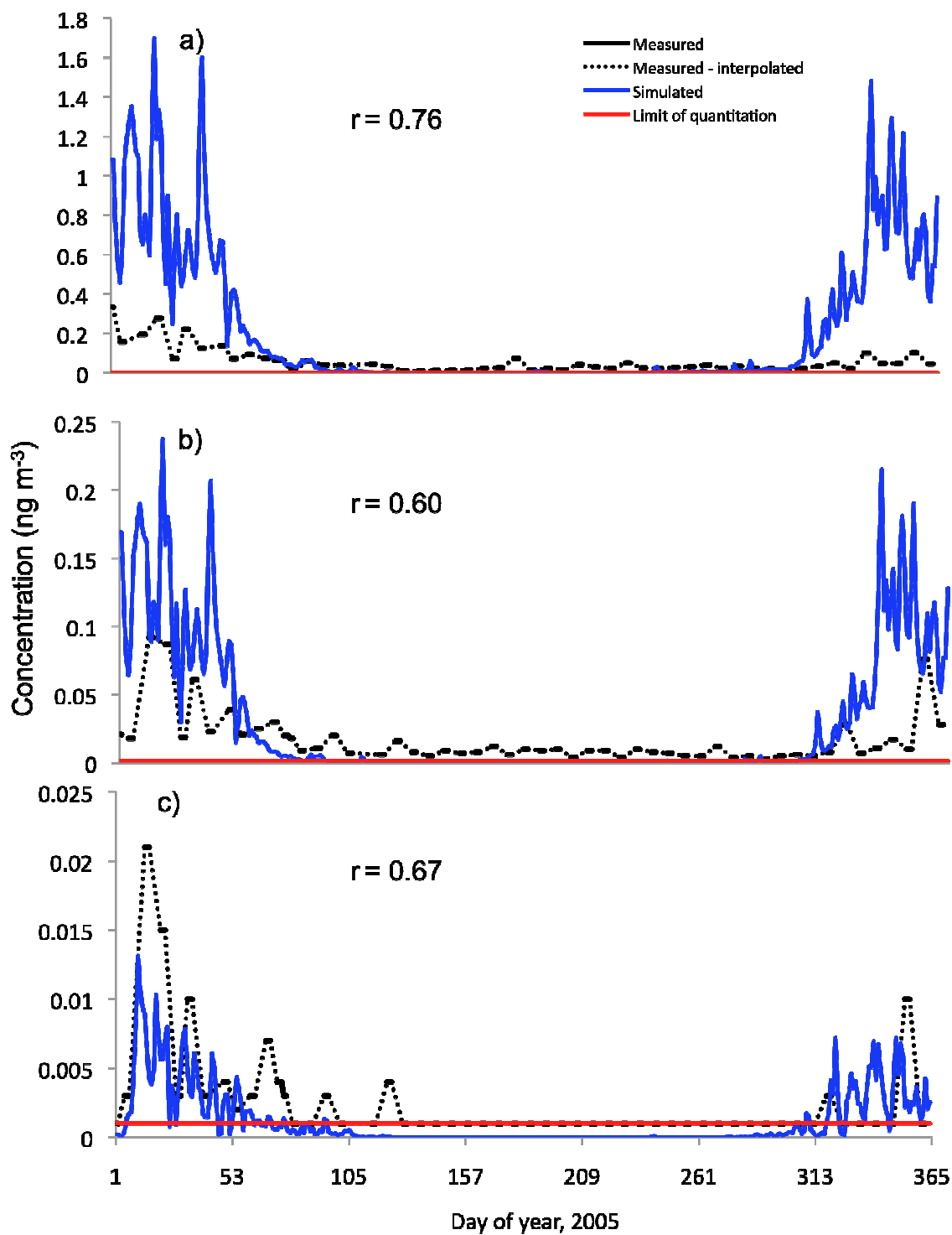


Figure S9. 2005 simulated and measured total a) PHE, b) PYR, and c) BaP at Spitsbergen, Norway.

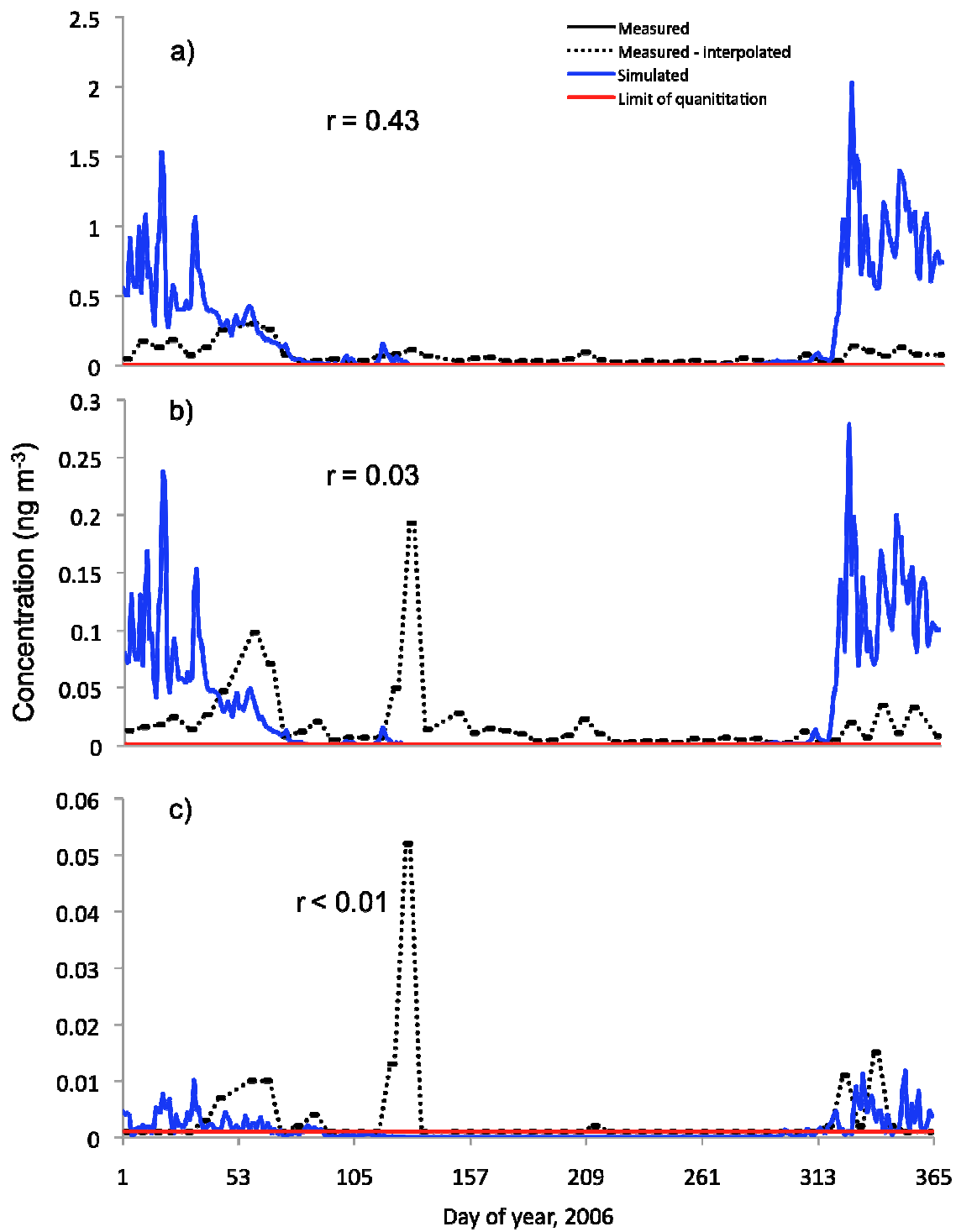


Figure S10. 2006 simulated and measured total a) PHE, b) PYR, and c) BaP at Spitsbergen, Norway.

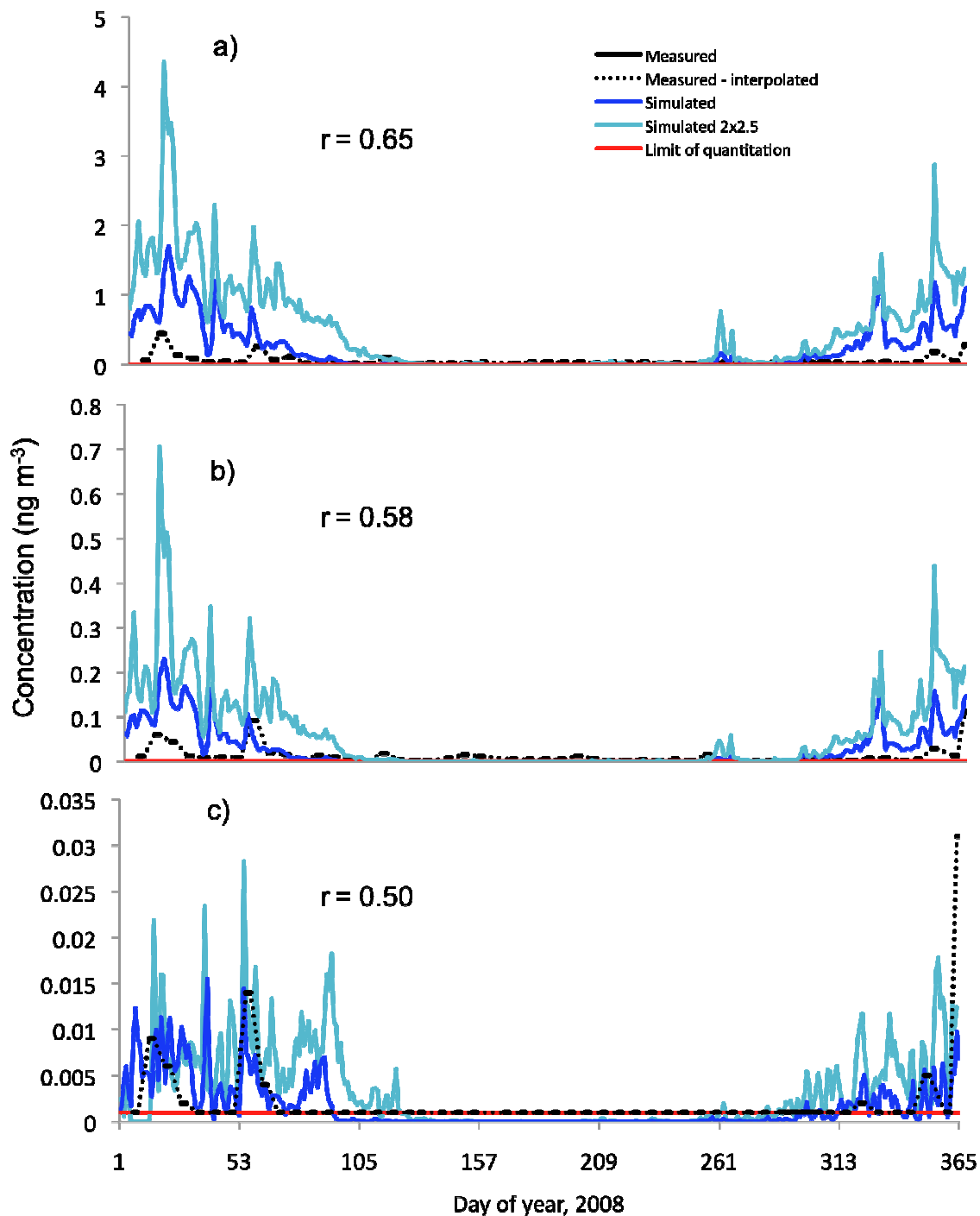


Figure S11. 2008 simulated and measured total a) PHE, b) PYR, and c) BaP at Spitsbergen, Norway. In addition, simulated concentrations at a $2^{\circ} \times 2.5^{\circ}$ spatial resolution are shown. Running the model at a finer spatial resolution results in increased plume concentrations, which are likely due to either a) decreased averaging of PAH plumes under a finer resolution, or b) decreased averaging of horizontal winds, which can result in weaker vertical transport and potentially less transport to Arctic regions⁹. The same effect is shown for 2009 simulations (below).

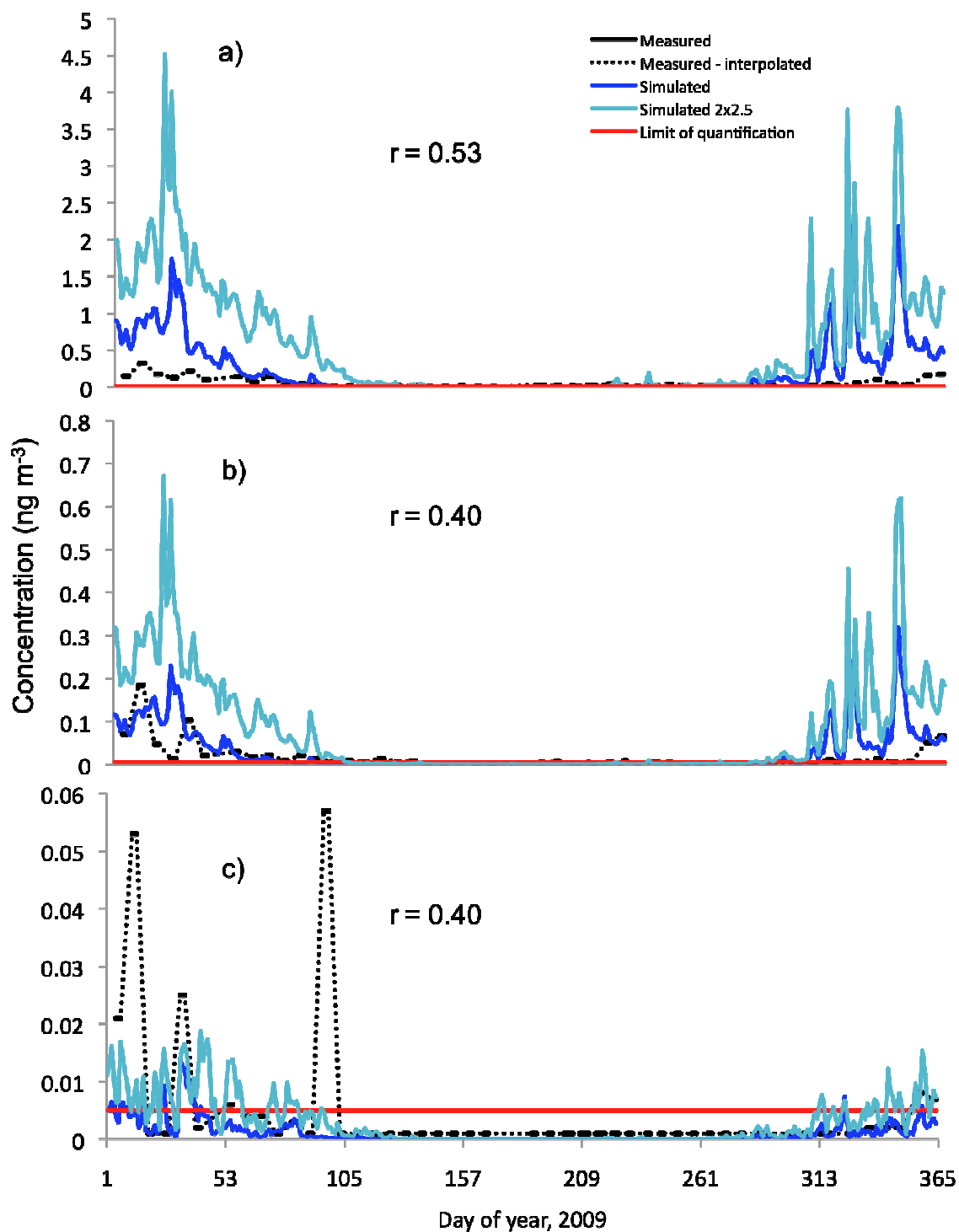


Figure S12. 2009 simulated and measured total a) PHE, b) PYR, and c) BaP at Spitsbergen, Norway. In addition, simulated concentrations at a 2°×2.5° spatial resolution are shown (see discussion in Figure S11 caption).

Literature Cited

1. Schwarzenbach, R. P.; Gschwend, P. M.; Imboden, D. M., *Environmental Organic Chemistry*. 2nd ed.; John Wiley & Sons: Hoboken, NJ, 2003.
2. Brubaker, W. W.; Hites, R. A., OH reaction kinetics of polycyclic aromatic hydrocarbons and polychlorinated dibenzo-p-dioxins and dibenzofurans. *J. Phys. Chem. A* **1998**, *102*, 915-921.
3. Pöschl, U.; Letzel, T.; Schauer, C.; Niessner, R., Interaction of ozone and water vapor with spark discharge soot aerosol particles coated with benzo[a]pyrene: O₃ and H₂O adsorption, benzo[a]pyrene degradation, and atmospheric implications. *J. Phys. Chem. A* **2001**, *105*, 4029-4041.
4. Kahan, T. F.; Kwamena, N.-O. A.; Donaldson, D. J., Heterogeneous ozonation kinetics of polycyclic aromatic hydrocarbons on organic films. *Atmos. Environ.* **2006**, *40*, 3448-3459.
5. Kwamena, N.-O. A.; Thornton, J. A.; Abbatt, J. P. D., Kinetics of surface-bound Benzo[a]pyrene and ozone on solid organic and salt aerosols. *J. Phys. Chem. A* **2004**, *108*, 11626-11634.
6. Ma, Y.-G.; Lei, Y.; Xiao, H.; Wania, F.; Wang, W.-H., Critical review and recommended values for the physical-chemical property data of 15 polycyclic aromatic hydrocarbons at 25 °C. *J. Chem. Eng. Data* **2010**, *55*, 819-825.
7. Lohmann, R.; Lammel, G., Adsorptive and absorptive contributions to the gas-particle partitioning of polycyclic aromatic hydrocarbons: State of knowledge and recommended parametrization for modeling. *Environ. Sci. Technol.* **2004**, *38*, 3793-3803.
8. U.S. EPA, Estimation Programs Interface Suite for Microsoft Windows, v 4.10. United States Environmental Protection Agency, Washington DC, USA. **2011**.
9. Wang, Y. X.; McElroy, M. B.; Jacob, D. J.; Yantosca, R. M., A nested grid formulation for chemical transport over Asia: Applications to CO. *J. Geophys. Res.* **2004**, *109*, D22307.